Vol. 22 No 3-II 2016

JOURNAL OF THE BALKAN TRIBOLOGICAL ASSOCIATION™®

Scientific Bulgarian Communications Ltd., Co.

CONTENTS

Vol. 22, No 3-II, 2016

Interdisciplinary aspects of trobilogy – flywheel energy storage system
V. G.MARIAN, T. LAURIAN, R.F. MIRCA, A. PASCU, P. SEICU. Theoretical and Experimental Analysis of Friction Forces Acting on a Flywheel Energy Storage System Rotating in Air 2175

Tribotechnics and tribomechanics
A. R. NIKOUEE, S. ADIBNAZARI. Crack Investigation in a Frame of a Passenger Airplane Structure Made of Aluminum Alloy 7075-T6 2186

Tribotechnics and tribomechanica – performance of elliptical journal bearings
PENG LIANG, CHANGHOU LU, FAZHAN YANG. Influences of Radical Clearance and Ovality on Performance of Elliptical Hydrostatic Journal Bearing 2198

Tribotechnics and tribomechanics – lateral slipping of vehicles tires
V. JIVKOV, PH. PHILIPOFF, N. NIKOLOV. Velocities in Contact Area of Turning Elastic Tires 2210

Tribotechnics – hybrid composites
R. ARRAVIND, M. SARAVANAN, A. BARADESWARAN, S. C. VETTIVEL, S. SURES. Tribological and Surface Behaviour of AA6061/Al2O3/Nano-graphite Hybrid Composite Using Casting 2218

Tribotechnics – regulation of rolling thickness on twin train
S. VULOVIC, N. JEVTIC, D. SPASIC, M. IVIC, Z. JANJIC, Z. ADAMOVIC. Mathematical Model of the System for Regulation of Rolling Thickness on Five Strands Twin Train 2227

Tribotechnics – mixed ferrite nanoparticles powder
C. RAMESH, K. MANIYSUNDAR, S. SELVANANDAN, P. M. ANBARASAN. XRD Structural and Magnetic Study on $Mg_{0.3}Zn_{0.7}Ni_XFe_{2-X}O_4$ Ferrite System Synthesized by Sol-Gel Method 2243

Tribotechnics – tribotesting and monitoring
LIN YONG-PING, ZHU FA-CAI, SHAO ZHEN-HUA, ZHANG HONG-YI. Characteristics of Partial Discharge on Typical Defects of 12 kV Power Transformers with Optical Fiber Based on Power Spectrum Density Methods 2252

Tribotechnincs and tribomechanics
J. H. TANG, K. Y. WANG, S. Y. BEI. Numerical Simulation of Electromechanical Composite Brake Based on Multi-Field Coupling 2265

Friction – dissipation effect
U. ARUNACHALAM, J. K. MANOJ, T. SIVAMARUGAN. Active Cooling System Design for Hypersonic Plane 2281

Frictional resistance – drag reduction characteristics
SHI YAO, PAN GUANG. Research on Drag Reduction Characteristics of Underwater Vehicle Fore Region with Short Groove Structures 2292

Wear of motor bearings
N. JANJIC, D. NIKOLIC, Z. JANJIC, B. SAVIC, B. CVETANOVIC. Determining Optimal Values Wear in Motor Vehicle Bearings 2308

Wear resistance increasing of mud pump by metal inert gas pulse-arc welding for surface cladding
M. B. IANCU, Vl. ULMANU, A. HADAR. Researches Regarding the Hardfacing Technologies of Mud Pump Valve Seats Applied for Increasing the Erosive Wear Resistance 2320

Wear rate – after cryogenic treatment of steel
K. AMINI, A. AKHABARIZADEH, A. ARAGHI. Investigating the Effect of the Deep Cryogenic Heat Treatment on the Corrosion and Corrosive – Wear Behavior of the Carburized 16MnCr5 Steel 2335

Computer simulations – contact and reflection
YONGCHENG LI, HAI SHEN, MANXI WANG. Multi-Objective Cognitive Radio Decision Engine Based on Autonomously Search Algorithm 2346

Computer simulations – technological tribological processes
ZEBIN YANG, LING WAN, ZHENG CHEN, XIAODONG SUN, LIN CHEN, PEIYU YU. Optimized Suspension Control of Bearingless Induction Motor Based on Auto-Disturbance Rejection Control 2363

Computer simulations
LI WENHUI, ZHANG LI, LI XIUHONG, YANG SHENGQIANG. Discrete Element Simulation of Particle Behavior in Mass Finishing Process: a Parametric Study 2380

Computer simulations – security risk forecast
NI ZHEN, LI QIANMUI, GANG LIU. Network Security Risk Forecast based on Markov Time-varying Model 2400

Computer simulations – reliability evaluation of smart grid
PENG-FEI LIU, QUN-TAI SHEN, QIU-FENG CHEN. Research on Reliability Evaluation of Smart Grid Based on Particle Reliability Algorithm 2417

Computer simulations
SHAOBIN HUANG, YA LI, YANMEI LI, DAPENG LANG, RONGHUA CHI. Fault Location Using Satisfiability in Complex Systems 2426

Design and calculations of tribosystems
A. SITTARAMANE, G.MAHENDRAN. Optimal Bonding Conditions for Diffusion Bonding of Aluminum Metal Matrix Composites Using Taguchi Based Response Surface Methodology 2437

Design and calculation of tribosystems
WU KE, FAN QINGLAI, HAO DONGXUE, CHEN RONG, LIU JINLONG. Construction Mechanics Effect of Submarine Immersed Tube Tunnel Subjected to Different Pore Pressures Based on Numerical Analysis 2447

Design and calculation of tribosystem
YUAN YUAN, WENJUN MENG, ZHENGMO YANG. Multi-objective Dynamic Optimisation of Gantry Crane Based on Reliability and Robustness 2454

Design and calculation of tribosystem – industrial articulated robots
S. A. AJWAD, A. MEHMOOD, M. I. ULLAH, J. IQBAL. Optimal V/S Robust Control: a Study and Comparison for Articulated Manipulator 2469

Design and calculation of tribosystems – artificial intelligence
YANG XIAOLEI, FENG YOUQIAN, YUAN XIUJIU, ZHAO XUEJUN. The Power of Natural Evolution in Solving Distributed Constraint Optimization Problems 2476

Disign and calculation of tribosystems – natural language processing
CHEN KEMING, ZHENG YIANGUO. Research on the Text Classification Based on Natural Language Processing and Machine Learning 2484

Vibration phenomena – railway gearbox faults
DECHEN YAO, JIANWEI YANG, XIAOQING CHENG, CHUNGQING ZHAO. Diagnosis of Railway Gearbox Faults Based on Wavelet De-Noising – Characteristic-Scale Decomposition – Particle Swarm Optimization – Least Squares Support Vector Machine 2495

Vibration phenomena – hydraulic turbine shafting
YIMING LI, GUIQIU SONG. Analysis of Bending Vibration of Bulb Hydraulic Turbine Shafting 2505

Vibration phenomena – vortex-induced vibration of tension leg platform
YOUGANG SUN, HAIYAN QIANG, DAOFANG CHANG, RAN WANG. Response Characteristic Analysis of Nonlinear Vortex-Induced Vibration of Tension Leg Platform in Deep Sea 2518

Vibration phenomena – tribotechnics and tribomechanics
QUANMIN GUO, DENGXIN HUA, LINGFEI KONG, ZHUYUAN FAN. Parallel Coordinating Control Strategy for Vehicle Magneto-Rheological Semi-Active Suspension 2535

Technological tribology – behaviour of high speed bearings
QIYIN LIN, BAOTONG LI, LUWEI ZHANG, HONG ZHAO, ZUOWEI WANG. Impacts of Surface Texture on the Tribological Behaviours of High-Speed Bearings 2553

Technological tribological processes
YANG LIU, LI LI, FAZHI SONG, JIUBIN TAN. Precision Motion Control of Motor Drive Systems with Actuator Nonlinearities and External Disturbances 2567

Tribochemical emissions – electrochemical behavior Ni^{2+} hexagonal mesoporous mesoporous lyophilic liquid crystal
A. A. AL-OWAIS, I.S. ELOHALLAG. Volta metric Investigations of Ni^{2+} in Hexagonal Lyotropic Liquid Crystaline Phase at Gold Disk Electrode 2583

Tribological properties determined by Taguchi method.
B. STOJANOVIC, M. BABIC, L. IVANOVIC. Taguchi Optimization of Tribilogical Properties of Al/SiC/Graphite Composite 2592

Biotribology – membranes and separators in microbial fuel cells
B. MIDYUROVA, V. NENOV. Novel Proton Exchange Membranes and Separators Applied in Microbial Fuel Cells (MFC) 2606

Biotribology – surface properties of dental alloys
KL. RADOMSKA, GR. PAWŁOWSKA, D. KLIMECKA –TATAR. The Influence of Current Density in the Electropolishing Process at the Stereometric Surface Properties of the Co-Cr Dental Alloys 2626

Biotribology
M. IVANOVA, I. MANOLOVA, M. GANEVA, R. GANCHEVA, R. STOILOV, S. STANILOVA. Elevated Serum Levels of TH17-Related Cytokines in Pateints with Ankylosing Spondylitis 2636

Lubrication – wall slip of spiral oil wedged sleeve bearings
LI-LI WANG, MIN WANG, XIAO-ZHEN DU, CHUN-JIAN SU. Experimental Investigation of the Wall Slip of a Low Viscosity Sleeve Bearing 2650

Lubrication – non continuum and dynamic effects of the lubrication film
CHEN QIAN, HUI WANG, YUANYUAN ZHU, YOINGBIN ZHANG. A Study on a Micro/Nano Step Bearing with Small Steps 2661

Lubrication – bush inner temperature in the presence of lubricants with different viscosity
LI-LI WANG, MIN WANG, XIAO-ZHEN DU. Temperature Characteristics of High Speed Sleeve Bearing with Two Viscosity Fluids 2676

Lubrication – cylindrical roller bearings film thickness
LI JUNNING, CHEN WEI. Skidding Analysis of High-Speed and Light-load Roller Bearing Based on Modified Film Thickness Formula and Considering Bearing Whirl with Elliptical Orbit 2688

Ecological tribology of fuels
M. JAMIL ABD ALGHANI. Evaluation Study of Different Types Adsorbents in Minimizing Sufur Contents in diesel Fuel 2704

Ecological tribology – biodiesel from micro algae
J. JAYAPRABAKAR, A. KARTHIKEYAN. Performance of Micro Algae Methyl Esters in a Compression Ignition Engine 2711

Role of tribology in sustainable developments
FAN CUN-HUI, QIN QI-RONG, OUYANG CHENG. Tectonic Fractures in Tight Sandstone Reservoirs of the Upper Creataceous Qingshaoukou Formation in Yaoyingtai Area of South-western Songliao Basin, China..... 2728

Role of tribology in sustainable development
KUNPENG LU, QIANG XIE, XIANG FU, ZHIWEI WANG, YI TANG. Analysis of the Mechanical Properties of Underground Circular Concrete Drainage Pipes 2745

Tribology of manufacturing processes – shape memory alloy
GE YANG*, SUN XIAOYU. Mechanical Performance of Aerated Block Walls With Shape Memory Alloy Reinforced..... 2757

Tribology of manufacturing processes – rapid identification of static stiffness
CHEN GUANGSHENG, ZHENG QINGZHEN. A Rapid Identification Method for Static Stiffness of Multi-Axis Cnc Machine Tools..... 2771

Management and organisation of production of red jujube
YI XIAOKANG, HU CAN, LI CHUANFENG, LI DAWEI, WU WENFU. Effect of Technological Parameters on Total Sugar Content of Red Jujube During Hot-Air Drying..... 2784

Management and organization of transport system
YAO CHEN , ALBIN, GU JIUCHUN, GAO CHAO. Research on Supply and Demand Non-Equilibrium Depth of City Agglomeration Transportation System 2795

Management of control strategies for tribosystems
TINGTING LIU, KAI CHEN, ZHIGANG YAN, QINGHUA MENG. Research on the Control Strategies of Vehicle Chassis Dynamometer..... 2803

Machinery breakdown
WANG XIULI, LU YONGGANG, ZHU RONGSHENG, FU QIANG, ZHONG WEIYUAN. Study of Non-Liner Cavitation on Flow Characteristics Inside The Centrifugal Pump 2826

Machinery breakdown – vehicle fatigue durability
YONGCHEN LIU, LI SUN. An Equivalent Coefficient Method Based on the Principle of Identical Fatigue Damage on Vehicle Structure 2843

Land sliding and land slipping – pre-splitting blast
LI XIANG-LONG, HU QI-WEN, MA XUE-BIN, LI KE-GANG, XIAO JIAN-QIANG. Experimental Research on Pre-splitting Blasting of the Final Highwall of an Opencast Coal Mine..... 2857

Land sliding and land slipping
WU KE, WANG YAJUN, LI SHUCHENG, ZAHNG WEN, WU HAOTIA. Study on Failure Mechanism of Expansive Soil Tunnel During Drying and Watering Cycle..... 2870

Land sliding and land slipping – tunnel support
JIANQING JIA, YONGPENG CUI, DONGSHENG XU, CHUNCHUN XIAO. Study on the Reliability of Tunnel Support Based on the Load and Structure Model..... 2879

Coatings – scratch test of chromium coatings
D. JOVANOVIC, B. NEDIC. Scratch Test of Chromium Coatings 2895

Aluminium metal matrix composites – lap shear strength in diffusion bonding
A. SITTARAMANE, G. MAHENDRAN. Process Parameters Optimization on Lap Shear Strength in Diffusion Bonding of Aluminium – Fly Ash (Afa) and Aluminium – Silicon Carbide (Asc) Composites Using Taguchi Method 2905

Nano-tribology – tungsten inert gas weld
PL. TASHEV, R. LAZAROVA, M. KANDEVA, R. PETROV, V. MANOLOV. Tungsten Inert Gas Weld Overlay Using Nano-sized Tin Powder 2914

Design and calculation of tribosystems – artificial intelligence
YANG XIAOLEI, YUAN XIUJIU, FENG YOUQIAN, ZHAO XUEJUN. Solving Distributed Constraint Optimization Problems Using Ant Colony Optimization 2931

3Dcolour printing device
CHUANFU HU, CAICHANG DING. A Color 3D- Printed Device and its Methods for Preparing 3D-Dimension Parts.... 2942

Journal of the Balkan Tribological Association Vol. 22, No 3, 2238–2254 (*2016*)

Nanotribilogy – tungsten inert gas weld

TUNGSTEN INERT GAS WELD OVERLAY USING NANO-SIZED TIN POWDER

P. TASHEV[a*], R. LAZAROVA[a], M. KANDEVA[b],
R. PETROV[c], V. MANOLOV[a]

[a] *Institute of Metal Science, Equipment and Technologies 'Acad. A. Balevski' with Hydro- and Aerodynamics Centre, BulgarianAcademy of Science*
67 Shipchenski Prohod Blv., 1574 Sofia, Bulgaria
[b] *Technical University of Sofia, 8 Kl. Ohridski 8, 1000 Sofia, Bulgaria*
[c] *Department of Materials Science and Engineering, Ghent University, 903 Technologiepark, Ghent, Belgium*

ABSTRACT

Automated tungsten inert gas (TIG) weld overlay was carried out on plates of low carbon steel S235JR (EN 10025) using nano-sized TiN powder coated with Cr (NM). Metallographic studies have been carried out on the microstructure of samples taken from the modified welds, as well as on control samples without nano-modifier. It was found that the use of nano-modifiers refines the average ferrite grain diameter in the welded overlay from 31 μm in unmodified samples to 15 μm in the samples with TiN nano-modifier. The comparison between the microhardness of the zones of the unmodified and modified weld metals showed up to 44% increased hardness in the modified samples. The ways of introducing of the nano-modifiers in the weld were discussed and conclusions are made concerning the effect of using nano-modifier on the structure and microhardness on the overlaid weld samples.
Keywords: TIG, weld overlay, additional wire, nano-modifier, TiN, modification.

INTRODUCTION

A new direction in material science related to use of nano- and micro-size particles for modification of metals and alloys has been recently developed[1-15]. The introduction of nano-sized particles in the molten metal results in formation of self-organising dispersion system. The solid particles surrounded by clustered lay-

* For correspondence.

ers serve as crystallisation nuclei in the micro-volumes of the suspension. Thus a heterogeneous system is created in which concentration over cooling occurs in the volume of the adsorbed layer that can substantially alter the process of structure formation and the quality of the metal. In the process of crystallisation it is the nano-particles that serve as nuclei for formation of solid phase. The nano-particles however have such nucleation properties only in case they have been pre-coated with an activated transitional layer. This layer ensures good wet ability of the particle from the melt and creates favourable conditions for growth of the solid phase on the particle surface even after small overcooling. The pre-coating to form such transitional layer can be made by means of either mechanical or chemical treatment in a planetary mill[2] or other methods for deposition of metal covers[16]. The experimental research evidences that both aluminum-and iron-based alloys have refined grain structure, better mechanical properties (strength and hardness) and improved wear resistance after modification with nano-particles[2-15]. However, there is still lack of data about nano-modification of welded overlays. The goal of the present work is to study the possibilities of implementation of nano-modification during welding and the corresponding microstructural – properties changes in the weld overlays after modification with nano- and micro- size particles.

EXPERIMENTAL METHODS

The present work aims to study the effect of using nano-sized TiN powder on the microstructure and the properties of overlaid weld layer of low carbon steel. As is known, nano-sized ceramic particles are not wetted well in contact with the liquid melt. For this reason it is necessary to cover them with a suitable metal to improve the wet ability. A mixture of nano-sized TiN powder with an average particle size of 70 nm and Cr powder with an average particle size of 44 nm is used in this work. A mechano-chemical activation of the mixture is performed using a planetary mill. A similar approach is used in Ref. 17.

Welding of the overlay. Plates with dimensions 250×120×3 mm of steel S235JR (EN 10025) with chemical content shown in *Table 1* were used in this work.

Table 1. Chemical content of steel S235JR

Chemical element	C_{max}	Mn_{max}	S_{max}	P_{max}	Si	N_{max}
%	0.17	1.40	0.040	0.040	0.15 – 0.25	0.012

The surfaces of the samples were cleaned by grinding and degreased before the welding of the overlay.

The weld overlay is carried out using pulse power source Fronius Magic Wave 2500 for TIG welding. The weld overlays were made with a welding speed of 96 mm/min, welding current of 100 A and voltage of 14 V. Protection atmosphere of inert gas Ar (BDS ENISO14175) designated as I 1was used with a consumption rate of 11l/min.

Welding wire for TIG welding designated as DT-SGMo (DIN 8576) with nominal diameter 1.6 mm was used in all experiments. The innovative technology for application of nano-sized powders on weld wire described in Ref. 1 is used. The procedure for application of nano-powder consists of several steps that ensure uniform distribution of the powder along the surface of the wire. The selected weld wire is coated with layer containing nano-modifier (NM) TiN +Cr and binds ing substance.

The test samples are weld overlaid in bottom position (PA) through tungsten inert gas (TIG) welding using as additional metal wire electrode which was pre-coated with a modifier containing nano-sized particles (TiN +Cr).

The weld overlay is carried out on a device with automated working movement of the welding torchand the additional metal was added manually – Fig. 1.

Fig. 1. Weld overlay with automated movement of the welding torch

The weld overlaid specimens are designated as follows:

- Sample 0: one overlaid layer using additional wire without NM;
- Sample 1: one overlaid layer using additional wire with NM;
- Sample 2: two overlaid layers using additional wire without NM;
- Sample 3: two overlaid layers using additional wire with NM.

The dimensions of the overlaid layers are 55×35 mm.

The process of weld overlay is recorded with an infra-red camera model Therma CAM SC640, (640×480 pixels), with possibility for measurements of temperature up to 2000 °C. The variation of the temperature field during welding different seams is recorded.

Methodology and device for testing the abrasion wear resistance. The methodology for testing of wear was developed by the authors and is based on measuring the mass wear of specimens for a certain road of friction at constantly set conditions – load, sliding speed and type of abrasive after which the characteristics are calculated: – speed wear, intensity of wear and abrasion wear resistance[18-23].

The experimental part of the methodology comprises the steps of:

– Preparation of samples with dimensions: 15×15 mm;

– Measuring the mass of the specimen m_0 using electronic scale WPS 180/C/2 with an accuracy of 0.1 mg. The specimen is cleaned from mechanical and organic particles before each measurement and dry with ethyl alcohol to prevent electrostatic effects;

– Fixing the specimen to the holder of the testers loading head, setting a specific normal load P and realising of certain road of friction;

– Measuring the mass m_i of the specimen after covering the given road of friction;

– Calculating the following characteristics (parameters) of mass wear:

Mass wear m, mg – ruined mass of the surface layer of the specimen for a certain road of friction L, i.e.

$$m = m_0 - m_i \,. \tag{1}$$

Wear-rate γ, mg/min – destroyed mass during friction per unit time of friction t:

$$\gamma = \frac{m}{t}. \tag{2}$$

Linear wear intensity i, μm/m is the change of specimen's height for unit sliding way:

$$i = \frac{m}{\rho A_a L} = \frac{h}{L} \tag{3}$$

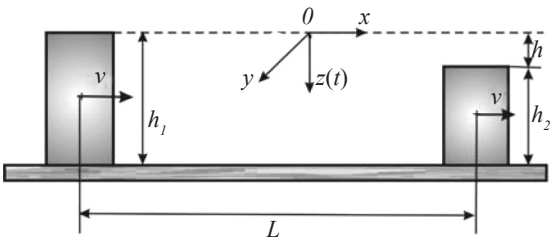

Fig. 2. Linear wear of the specimen after given sliding way

where ρ is the density of the surface layer of the sample, A_a –nominal (geometric) contact area.

Linear wear resistance I, m/μm is expressed as reciprocal value of the wear intensity:

$$I = \frac{1}{i} = \frac{\rho A_a L}{m} = \frac{L}{h}. \tag{4}$$

And is a quantity showing the length of the sliding way L traveled by the specimen under the given conditions of friction, so that the decrement of the height h will be 1 μm. Most of ten linear wear resistances are given by a dimensionless value, i.e. [m/m] instead of [m/μm].

Comparing in respect to the indicator 'wear' is performed under the same test conditions.

Abrasion during dry friction is examined with device according kinematics scheme 'pin-on-disk' whose functional design is shown in Fig. 3.

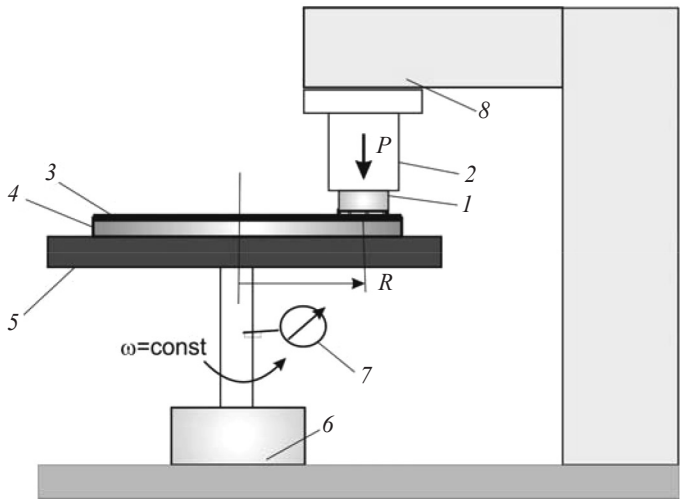

Fig. 3. Functional scheme of tribotester 'pin-on-disk' for testing of abrasive wear

The examined coated sample *1* (finger) is firmly attached in the groove of the holder *2* of the loading head *8* in a manner that the coated surface contacted withthe abrasive surface of the horizontal disk *4*. The disk is driven by electric motor *6* and revolves around its vertical axis with angular velocity ω=const.

The normal load *P* is applied in the centre of gravity of the area of contact between the sample and the abrasive surface and is weighed via lever system position with in the loading head. The road friction is defined by the number of revolutions of the cyclometer *7* and is calculated using the formula $L=2\pi RN$, where *R* is the distance between the axis of revolution of the disk *4* and the axisof the sample *1*, and *N* is the number of cycles of abrasion. The nominal contact pressure is calculated using the formula: $p_a = P/A_a$.

The abrasion surface *3* is impregnated corundum (E) with hardness 9.0 on the Moos scale that meets the requirement for at least 60% higher hardness thanthat of the tested material.

The experimental conditions are given in Table 2.

Table 2. Parameters of the testing for wear resistance

Load	P = 4.53 N
Aparent contact area $A_a = 225.10^{-6}$ m^2	
Aparent contact area	p_a = 0.2 MPa
Sliding speed	V = 13.1 cm/s
Abrasive surface	corundum P 120

Microstructural characterisation. The specimens for metallographic and microhardness analyses were cut off by water jet from the central zone of the weld overlay and prepared following the standard procedures – Fig. 4. The macrostructure was revealed with 10% solution of ammonium per sulfate in water and for revealing the microstructure 4 vol. % solution of nitric acid in ethanol was used. The microstructure is characterised by means of optical metallographic microscope PolyvarMet equipped with digital camera.

Figure 4 shows double weld overlaid layer with additional wire with nano-modifier in binding substance (sample 3). The rectangular zones from where the samples for microstructural analysis were cut are clearly visible.

Electron backscatter diffraction analysis (EBSD) was carried out on the cross section of the specimens on a distance of ~100 μm from the top surface of the weld. EBSD data were acquired on FEI Quanta 450 SEM with a field emission gun, operating at 20 kV, working distance of 16 mm and a beam corresponding to FEI spot size # 5. The samples for EBSD were mechanically ground and polished to final polishing step of 1μm and next polished by means of A2 Struers ® elec-

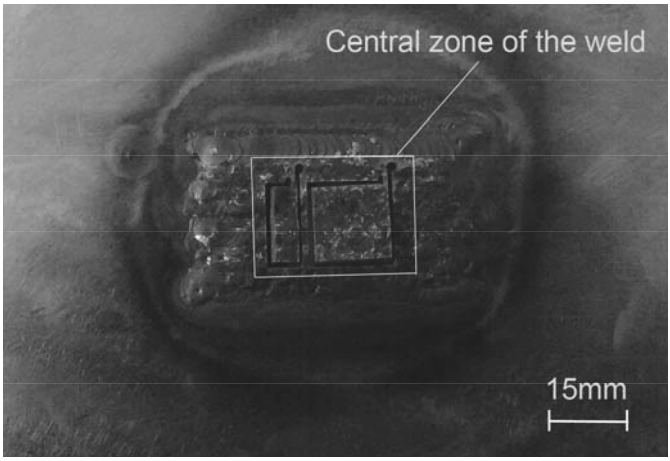

Fig. 4. Sample 3 – double weld overlaid specimen with additional wire with nano-modifier

trolyte at room temperature (22°C), 40 V for 10 s. EDAX- TSL Data Collection v.6 software was used for EBSD data acquisition with step sizes of 1.5 μm and 0.5 μm (depending on the magnification) in hexagonal scan grid. The EBSD data were post-processed by means of TSL-OIM data Analysis v.6.2 software. Raw data were cleaned up to remove the points with low indexation reliability (CI<0.1) which in the worst cases did not exceed 5% of total number of points in the scan.

Micro hardness of the samples was measured using Vickers micro hardness measuring device Duromat 4000 with 50 g load and duration of 10 s.

The measurements were made on a distance of 1 mm from the overlaid surface – Figs 5 and 7. It is assumed that the thermal cycles at these zones of the samples are identical in all samples and hence the differences in the microstructure and the hardness can be associated only to the influence of the nanomodifiers.The results from the measurements are shown in Table 3.

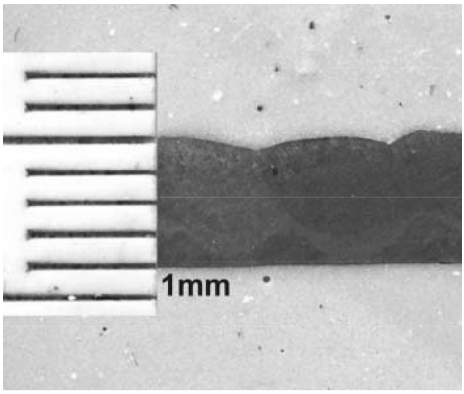

Fig. 5. Macrostructure in the cross section of a weld overlaid layer on plate, sample 3 (2 layers, with nanomodifier). One division of the scale bar is 1 mm

Table 3. Wear parameters of the reference samples No 0 – 3

1.	Cycle number	50	100	150	200
2.	Sliding time (min)	0.24	0.48	0.72	0.96
3.	Sliding way (m)	11.3	22.6	33.9	45.2
Sample No 0					
4.	Mass loss (mg)	6.2	12.5	15.4	17.5
5.	Wear rate (mg/min)	25.8	26.04	21.4	18.23
6.	Wear Intensity (m/m)	3.3×10^{-6}	3.1×10^{-6}	2.57×10^{-6}	2.2×10^{-6}
7.	Wearresistance (m/m)	0.3×10^{6}	0.32×10^{6}	0.39×10^{6}	0.45×10^{6}
Sample No 1					
4.	Mass loss (mg)	3.4	5.3	6.1	8.4
5.	Wear rate (mg/min)	14.2	11.04	8.47	8.75
6.	Wear Intensity (m/m)	1.7×10^{-6}	1.3×10^{-6}	1.01×10^{-6}	1.05×10^{-6}
7.	Wearresistance (m/m)	0.59×10^{6}	0.76×10^{6}	0.99×10^{6}	0.95×10^{6}
Sample No 2					
4.	Mass loss (mg)	3.7	10.2	13.8	18.3
5.	Wear rate (mg/min)	15.4	21.2	19.2	19.1
6.	Wear intensity (m/m)	1.85×10^{-6}	2.52×10^{-6}	3.2×10^{-6}	2.39×10^{-6}
7.	Wearresistance (m/m)	0.54×10^{6}	0.4×10^{6}	0.31×10^{6}	0.42×10^{6}
Sample No 3					
4.	Mass loss (mg)	2.4	5.3	8	11.6
5.	Wear rate (mg/min)	10	11	11.1	12
6.	Wear intensity (m/m)	1.2×10^{-6}	1.3×10^{-6}	1.33×10^{-6}	1.45×10^{-6}
7.	Wearresistance (m/m)	0.83×10^{6}	0.75×10^{6}	0.75×10^{6}	0.7×10^{6}

RESULTS AND DISCUSSION

Temperature field. Figure 6 shows the temperature field in the area of weld overlay of the seam at point corresponding to time τ=16 softer the beginning of the welding process, as well as the variation of the temperature as a function of time in point Sp1 of the overlaid area. The chosen point is located within the heat affected zone close to the line of fusion in the overlay weld. It is seen from the graph that the temperature in this point reaches maximum of 1050°C. The average heating rate of the surface of the overlaid weld in the linear part of the curve is 183 °C/s, and the average cooling rate is 75 °C/s.Similar data are acquired for any point of the overlaid weld for either single or double layer.

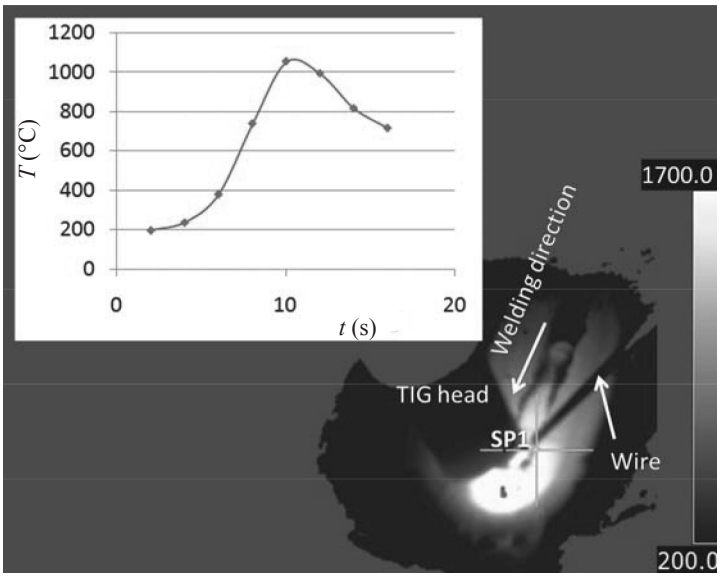

Fig. 6. Temperature filed in the area of weld overlay acquired with infrared camera and temperature–time dependence in selected point Sp1 within the area

It is seen from the image that due to the double layer weld overlay, the structure of the specimen is changed throughout the whole depth.

Microstructure characterisation. The microstructure of the base metal in all studied specimens is ferrite with equiaxed grains and lamellar pearlite. The micro hardness is almost the same in all samples, i.e.155–159 kg/mm^2. However sample No 3 has slightly higher micro hardness indicating that the base metal probably has been influenced by the multiple welding.

The results from microhardness measurements of the specimens are compared graphically in Fig. 9.

A single layer welded sample without nano-modification (sample 0) has ferrite and pearlite microstructure of the overlay. The pearlite is uniformly distributed and after the weld overlay the grains have equal axed shape. The microstructure of the overlay does not differ significantly from the microstructure of base metal. The slightly increased microhardness of the layer might be associated to the residual stresses after welding.

The microstructure of the overlaid layer of sample 1 is also ferrite and pearlite. The pearlite does not show clearly separated colonies and could be associated to sorbate – Fig. 7; Pearlitic strips (extended pearlitic colonies) are also observed in this sample. The microhardness of the single overlaid layer with NM is 239 $HV_{0.05}$ which is with 44% higher than that the hardness of the sample without nano-modification (sample 0).

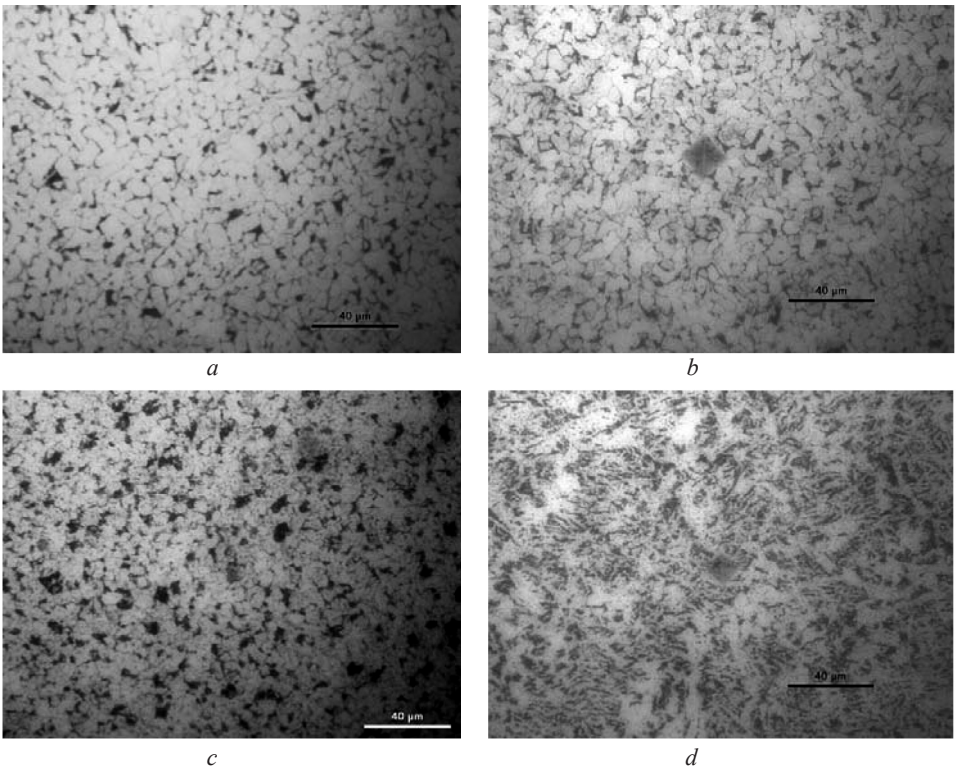

a *b*

c *d*

Fig. 7. Single-layer weld overlaid specimens with/without NM: (*a*) sample 0, base metal; (*b*) sample 0, weld overlay without NM; (*c*) sample1, base metal; (*d*) sample 1, weld overlay with NM

Ferrite and needle-shaped pearlite organized in Widmannstätten type structure are the characteristic features of the microstructure of the welded overlay of sample 2. The average length of pearlite colonies in this specimen is 14.5 µm and the average width is 2 µm. Microhardness on the overlaid zone is increased to 220 $HV_{0.05}$, i.e. the increase in hardness is 39% in comparison with the base metal. That increase in microhardness is due to both, changes in the morphology of the microstructure and the residual stresses in this zone as a result of the weld overlay.

After the weld overlay of sample 3, the layer has homogenous microstructure of fine grain pearlite of average size pearlite colony of 0.6 µm, Fig.8 which means that the refinement of pearlite is about 91% in comparison to the base metal. The layer in specimen No 3 has microhardness 282 kg/mm^2, which is with 71% higher than that of the base metal and 28% higher than that of the overlaid metal in sample 2 which is without nano-modification of the weld. Several microstructure strengthening mechanisms could play a role for increasing the hardness in this

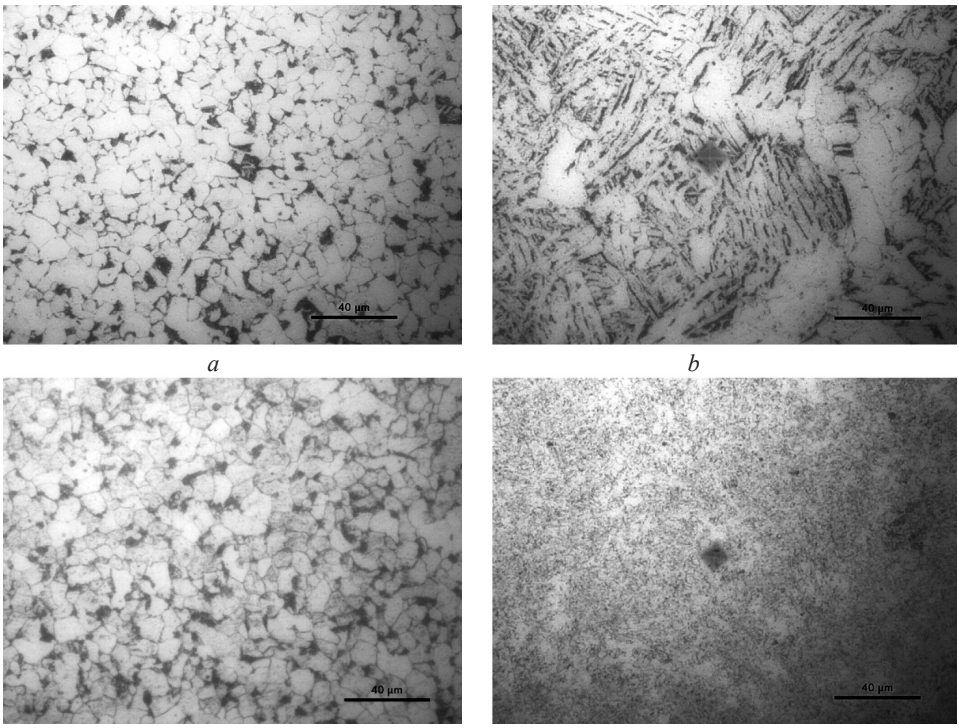

Fig. 8. Double-layer weld overlaid welded specimens with/without NM: (*a*) sample 2, base metal; (*b*) sample 2, weld overlay without NM; (*c*) sample 3, base metal; (*d*) sample 3, weld overlay with NM

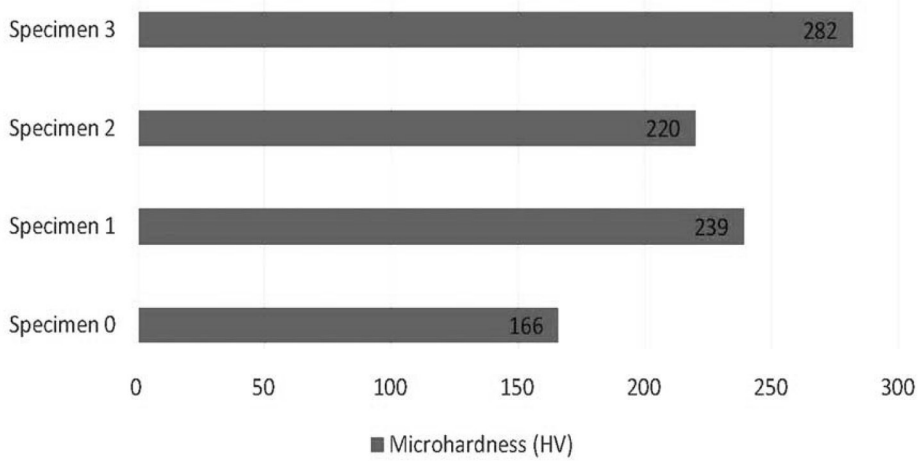

Fig. 9. Comparison of Vickers microhardness of specimens measured with loading 50 g and duration 10 s

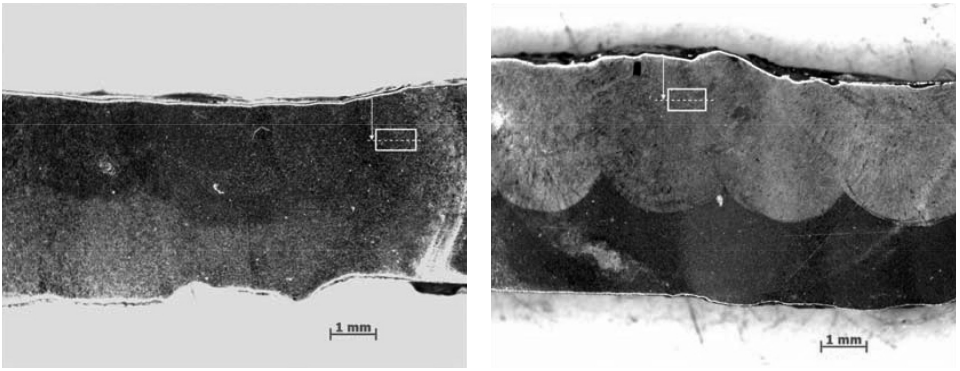

Fig. 10. Sample 3: a) without nano-modification and b) sample 3 with nano-modification, on which the zones of the EBSD measurement are marked with white rectangles

zone: (i) grain refinement due to modification with nano-particles; (ii) generation of internal stresses due to weld thermal cycle and (iii) possibly precipitation hardening.

EBSD measurements were carried out on the surfaces shown in Figs 10 *a*, *b* on a distance of 1 mm under the surface in order to correspond exactly to the zones where the microhardness was measured.

The results of the EBSD analysis of samples without and with nano-modification are shown in Figs 11 *a* and *b* correspondingly. The microstructure in the modified layer Fig. 11 *b* consist of fine equal axed grains with an average grain diameter of 15 μm, whereas the microstructure of the sample taken from the similar place from unmodified sample Fig. 11 *a* contains acicular ferrite and pearlite with large elongated grains with an average calculated diameter of 31 μm. The distribution of the average grain size calculated on the base of 5° disorientation between the neighbouring pixels and minimum 4 pixels per grain is shown in Fig. 12. All points with a confidence index lower than 0.1 are excluded from the data quantification as dubious. These points appear in black in the colour coded maps and were not counted in the grain size calculation. The EBSD data show that the nano-modification changes not only the grain size but influences significantly the grain morphology. Figures 11 *c* and *d* display high resolution EBSD maps of the zones from Figs 10 *a* and *b*. It is clear that the pro-eutectoid ferrite on the prior austenite grain boundaries Fig. 11 *c* is replaced by ferrite with acicular morphology Fig. 11 *d* in the alloy with addition of nano-particles.

Key for orientation coding is shown in the right upper corner as an unit triangle.

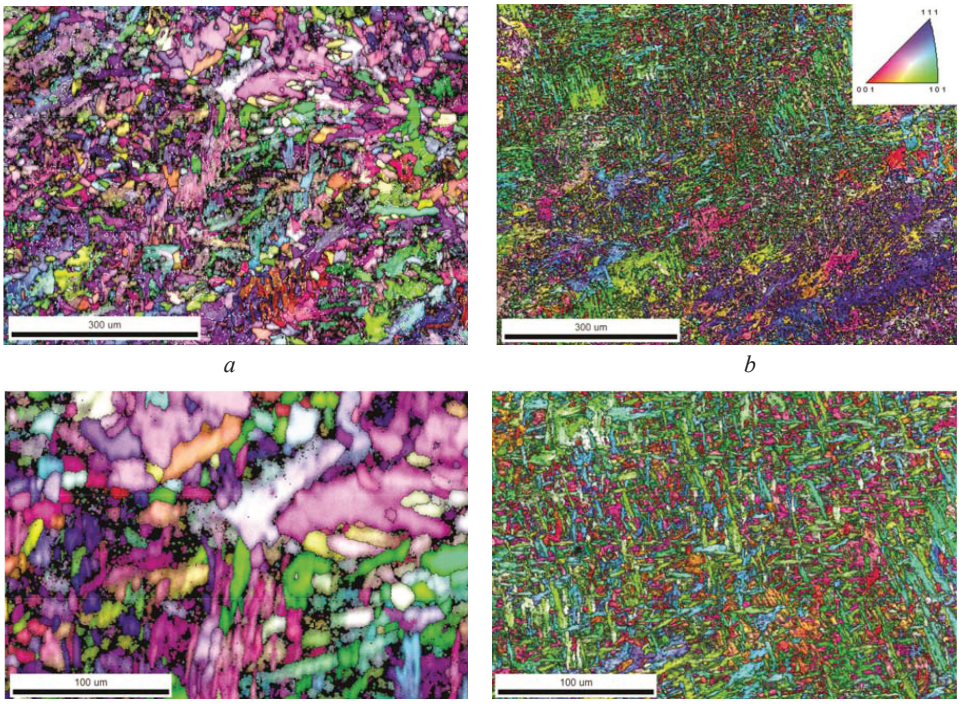

Fig. 11. Combined Image quality and normal direction inverse pole figure maps from sample: (*a*) without modification, (*b*) with modification. Detailed view of the zones from samples: (*c*) without modification, (*d*) after modification

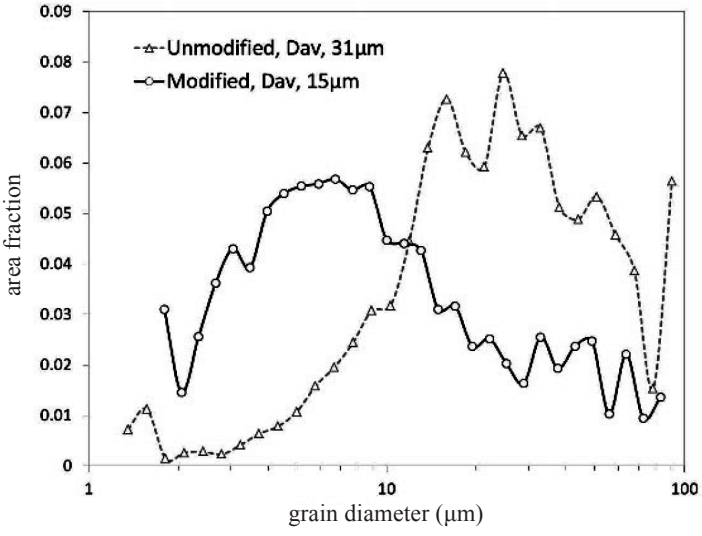

Fig. 12. Distribution of the average grain diameter (area fraction) of the grains in the subsurface layers for modified and unmodified structures

Study of wear resistance. Characteristics of abrasion and wear resistance of nanomodified samples and the reference sample.

The results obtained for the characteristics of abrasion and wear resistance of all examinedamples for different paths offriction are shown in Table 3.

The relative wear resistance of samples in comparison with the base sample (No 0) one is shown in Table 4 and Fig. 13.

Table 4. Relative wear resistance

Relative wearresistance $E_{i,e} = I_0$ for N = 200 cycles			
E_0	$E_{1.0}$	$E_{2.0}$	$E_{3.0}$
1.0	2.1	0.93	1.56

The results show that as a consequence of single layer weld overlay with nanomodifying the relative wear resistance increases with 210%. In two-layer weld overlay with nanomodifying it increases with 156% compared to the base sample single-layer weld overlaid without nanomodifying. Less effect of improving the wear resistance in two-layer welding with nanomodifying the liquid phase is probably due to excess of concentration of nano modifiers in the overlaid layer above a certain threshold level which is recommended to be established with further researches on the impact of the concentration of nano modifiers on the

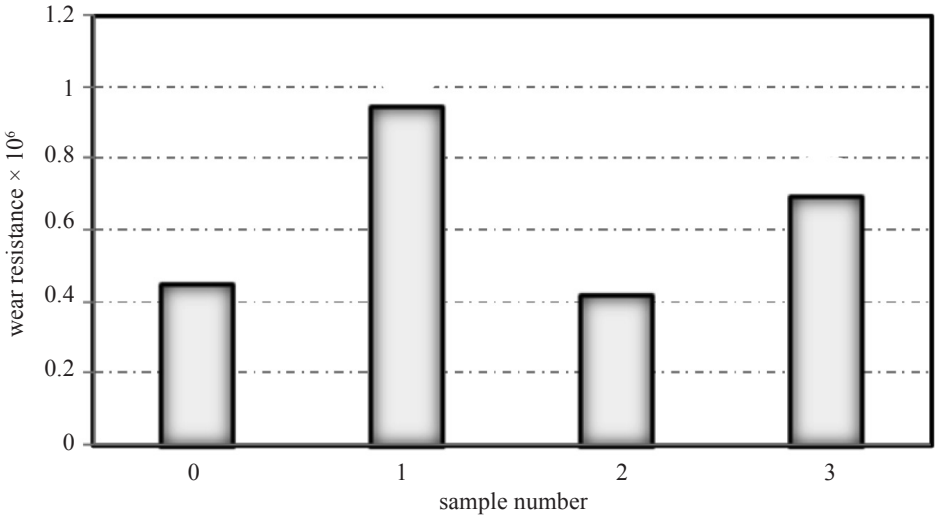

Fig. 13. Diagrams of the linear wear resistance of the tested specimens

abrasion resistance. For practical impact of the increasing durability of 210%. It has a significant economic impact, taking into account the saving of energy and materials in the use of single-layer instead of two-layer weld overlaying.

The impact of the increasing wear resistance with 210% a significant economic impact for the practice taking into account the saving of energy and materials in the use of single-layer instead of two-layer welding.

CONCLUSIONS

1. TIG weld overlay with introduction of nano-size TiN powder embedded in coated electrode wire was applied on a low carbon steel grade to study the effect of the nano-particles on the properties of weld overlaid layers.

2. The comparison between microstructures of single-layer overlaid weld with and without nano-modifier revealed the presence of ferrite-pearlite structures in both cases. In the modified specimen however, the pearlite refines and its morphology changes from lamellar with separate grains towards sorbite-like one.

3.Double-layer overlaid welds with or without nano-modifiers displayed always microstructure of ferrite and pearlite. However in the unmodified samples lamellar pearlite colonies with average dimensions of 14.5×2 μm were present whereas nano-modification refined the average size of pearlitic colony to 0.6 μm. Expresed in persentage the pearlitic colonies after modifications are 91% smaller than that of the unmodified specimen.

4. Nano-modification changed the ferrite morphology to acicular and decreases the average grain diameter from 31 to 15μm in the samples with double-layered overlays.

5. The microhardness in nano-modified specimens is 44% higher for single-layer weld and 28% for double-layer weld in comparison to unmodified samples with the same number of layers.

6. The relative wear resistance increases with 210% after single layer weld overlay with nanomodifying.

ACKNOWLEDGEMENTS

This study is financed by BSMEPA by means of the National Innovation Fund under Contract No 6IF 02-35/15.12.2012.

REFERENCES

1. P. TASHEV, T. PETROV, Y. LUKARSKI, G. STEFANOV: Technologies for Introduction of Nano-Sized Particles in the Weld in Processes of Overlaying Welding. Engineering Sciences, (**3**), 82 (2013).
2. V. SABUROV, E. EREMIN, A. CHEREPANOV, G. MINNEKHANOV: Modification of Steels and Alloys by Dispers Inoculators. Izd. OmGTU, Omsk, 212 (2002).
3. ZD. KARAGUIOZOVA, V. MANOLOV, M. TARASOV: Elektroless Iron Coating on Nano-sized Particles. BULTRIB'11 – 8th National Conference on Tribology with International Participation, Sofia, 28.10.2011, Tribological Journal BULTRIB, **2**, 73 (2012).
4. N. KALININA, O. KAVATZ, V. KALININ: Airspace Technique and Technology, **4**, 17 (2010).
5. N. KALININA: Nanomaterials and Nanotechnologies: Obtaining, Structure, Application, Dnepropetrovsk, Publishing Hous U.V. Makovetskiy, pp. 2012.
6. R. LAZAROVA, R. PETROV, V. GAYDAROVA, A. DAVIDKOV, A. ALEXEEV, M. MANCHEV, V. MANOLOV: Microstructure and Mechanical Properties of P265GH Cast Steel, After Modification with Ticn Particles. Materials and Design, **32**, 2734 (2011).
7. R. LAZAROVA, P. KUZMANOV, R. DIMITROVA, A. CHEREPANOV, V. MANOLOV: Properties of 110Г13L {Cyrillic} Steel and Sch 25 Cast Iron Modified By Refractory Nanopowder, Steel in Translation, **42**, Issue 4, 298 (2012).
8. P. KUZMANOV, R. DIMITROVA, R. LAZAROVA, A. CHEREPANOV, S. POPOV, R. PETROV, V. MANOLOV: Investigation of The Structure and Mechanical Properties of Castings of Alloy AlSi7Mg, Cast Iron GG15 and GG25 and Steel GX120Mn12, Modified by Nano-sized Powders. Proceedings of the Institution of Mechanical Engineers, Part N: Journal of Nanoengineering and Nanosystems, **228**, 1, 11 (2014).
9. M. RAZAVI, M. RAHIMIPOUR, A. RAJABI-ZAMANI: Effect of Nanocrystalline TiC Powder Addition on the Hardness and Wear Resistance of Cast Iron. Materials Science and Engineering A, **454-455**, 144-147 (2007).
10. R. DIMITROVA, P. KUZMANOV, R. LAZAROVA, V. MANOLOV: Investigation of Nanopowders Application in Metal Casting. Advanced Materials Research, **629**, 284.
11. K. BORODIANSKIY, M. ZINIGRAD, A. GEDANKEN: Aluminum A356 Reinforcement by Carbide Nanoparticles. Journal of Nano Research, **13**, 1 (2011).
12. K. BORODIANSKIY, A. KOSSENKO, M. ZINIGRAD: Improvement of the Mechanical Properties of Al-Si Alloys by TiC Nanoparticles. Metallurgical and Materials Transactions A, **44**, 4948 (2013).
13. M. HABIBNEJAD-KORAYEM, R. MAHMUDI, W. J. POOLE: Enhanced Properties of Mg based Nano-Composites Reinforced With Al_2O_3 Nano-Particles. Mater *S*ci Eng A, **519**, 198– (2009).
14. M. HABIBNEJAD-KORAYEM, R. MAHMUDI, H. M. GHASEMI, W. J. POOLE: Tribological Behavior of Pure Mg and AZ31 Magnesium Alloy Strengthened by Al_2O_3 Nanoparticles. **268**, 405 (2010).
15. Y. HOU, Y. WANG, Z. PAN, L. YU: Influence of Rare Earth Nanoparticles And Inoculants on Performance and Microstructure of High Chromium Cast Iron. Journal of Rare Earths, **30**, 283 (2012).
16. S. STAVREV, Z. KARAGUIOZOVA: Formation of Nickel Layer – Covers on Nanodiamond Powder. Nanoscience&Nanotechnology, **7**, 219 (2007).
17. JIN-JU PARK, SUNG-MOHONG, EUN-KWANG PARK, KYONG-YEOLKIM, MIN-KU LEE, CHANG- KYU RHEE: Microstructure and Properties of SA106B Carbon Steel after Treatment of the Melt with Nano-Sized TiC Particles. Materials Science & Engineering, A613, 217 (2014).

18. V. PETKOV, P. TASHEV, N. GIDIKOVA, M. KANDEVA, R. VALOV: Wear Resistant Chromium Coating With Diamond Nanoparticles Upon an Arc Deposited Layer. J Balk Tribol Assoc, **21** (1), 134 (2015).
19. M. KANDEVA: The Contact Approach in Engineering Tribology, Technical University – Sofia. 504 (2012).
20. M. KANDEVA, D. KARASTOYANOV, B. IVANOVA, A. DIMITROVA, Y. SOFRONOV, N. NIKOLOV: Friction and Wear of Ni Coatings with Nanosize Particles of SiC. 5th World Tribology Congress (WTC 2013), Turin (Italy), 08-13.09.2013, Proceedings, Paper 1241.
21. M. KANDEVA, B. IVANOV: Abrasive Wear and Wear Resistance of High Strength Cast Iron Containing Sn Microalloy. J Balk Tribol Assoc, **19**(4), 584 (2013).
22. M. KANDEVA, A. VENCL, E. ASSENOVA, D. KARASTOYANOV, T. GROZDANOVA: Abrasive Wear of Chemical Nickel Coatings with Boron Nitride Nano-Particles. 11th International Conference in Manufacturing Engineering the "A" Coatings, Thessaloniki (Greece), 01-03.10.2014, Proceedings, 319-325.
23. M. KANDEVA, AL. VENCL, D. KARASTOYANOV: Advanced Tribological Coatings for Heavy-Duty Applications: Case Studies, Marin Drinov, Academic Publishing House, Sofia, 2016.

Received 9 March 2016
Revised 15 April 2016